Towards domestic cooking efficiency: A case study on burger pan frying using experimental and computational results

E. Hernández-Alhambra [a], P. Guíu [b], I. Cabeza-Gil [a], A. Ferrer-Mairal [b], M.A. Martínez [a,c], B. Calvo [a,c], J. Grasa [a,c,*], M.L. Salvador [b]

[a] *Aragón Institute of Engineering Research (i3A), Universidad de Zaragoza, Spain*
[b] *Plant Foods Research Group, Instituto Agroalimentario de Aragón IA2, Universidad de Zaragoza-CITA, Miguel Servet 177, 50013 Zaragoza, Spain*
[c] *Centro de Investigación Biomédica en Red en Bioingeniería, Biomateriales y Nanomedicina (CIBER-BBN), Spain*

ARTICLE INFO

ABSTRACT

It is well known that the use of efficient domestic cooking appliances and equipment can not only save energy, but also improve the quality of the food being prepared. This work raises the question of whether cooking procedures can also contribute to this energy efficiency. Focusing on burger pan frying, experimental data were used to develop a model able to predict cooking outcomes under different power levels supplied by an induction hob. The proposed model takes into account not only the heat consumed by water evaporation in the contact region but also the shrinkage process of the hamburger. A new formulation based on the multiplicative decomposition of the strain deformation gradient is proposed to describe the observed decoupling between weight and volume loss during the process. The model properly predicts temperature, moisture loss and shrinkage, and allows elucidation of the effects of supplying different amounts of energy on the final water content.

1. Introduction

Improving the efficiency and sustainability of food processing involves the important challenge of optimizing commercial cooking devices for better energy use and transmission. The development of computational models has become an important tool for this purpose (Datta et al., 2022; Erdogdu, 2023). These models have the potential to reduce the use of resources in the design stages but also to provide a better knowledge of the complex transformations that food undergoes. Moreover, models related to meat cooking processes can help to select cooking conditions that allow high energy efficiency (Thiffeault, 2022), define scenarios for ensuring microbiological safety (Ou and Mittal, 2006, 2007), and help to obtain a product with the highest degree of denaturation of myosin and collagen proteins, and the lowest degree of actin denaturation and weight loss (Szpicer et al., 2022), in order to achieve good sensory attributes such as tenderness and chewiness (Erdogdu et al., 2005).

Unlike what happens in the industrial processes or in out-of-home catering, efficiency in the domestic cooking of hamburgers is not linked to obtaining a certain temperature in the centre of the burger in the shortest possible time, but rather to obtaining a product of good quality. The process should not compromise the quality of the product by producing excessive temperatures on the surface in contact with the pan,

which would result in the formation of an excessively brownish and tough crust, and the consequent production of compounds potentially harmful to health - PAHs, HAA and acrylamide (Onopiuk et al., 2021). Microbiological safety in hamburger cooking is determined by the need to avoid the well known disease caused by *Escherichia coli* O157:H7 and the presence of other pathogens such as *Listeria monocytogenes* and *Salmonella* serotypes (Liu et al., 2023). The US Department of Agriculture (USDA, 2016) recommends reaching a minimum of 160 °F (71.1 °C) for ground meats to enhance food safety. Gastronomically, a sufficiently high pan temperature is recommended so that the Maillard reaction is accelerated and flavour and colour develop quickly (McGee, 2004; Myhrvold et al., 2011). Studies on the influence of this pan temperature differ between considering its effect on the development of the hamburger core temperature negligible (Dagerskog, 1979), to concluding that an increase in the pan temperature from 180 to 200 °C results in a rise in the core temperature from 68.4 to 83.1 °C, for the same cooking time (Pan et al., 2000). Furthermore, a 39 % increase in cooking time was observed when the pan temperature was reduced from 175 to 100 °C, to achieve the same central temperature (Oroszvári et al., 2005a). Events during burger cooking, such as the helix-coil transition of collagen and the myosin and actin denaturation, induce the collapse of the protein matrix, with the consequent loss of water

---

retention capacity and increase in hardness and shrinkage (Vu et al., 2022).

The cooking process of meat hamburgers involves physical phenomena that can be described in a modelling framework that includes energy transport, mass transport and deformation in a porous media (Datta, 2007; Khan et al., 2016; Zorrilla and Singh, 2003). These phenomena have been integrated in different ways and detailed in several models. Some of them include heat transfer and diffusive transport for moisture using an experimentally determined effective diffusivity (Shilton et al., 2002). During cooking, the contraction of the protein network exerts a swelling pressure that leads to the expulsion of moisture from the meat. This has been described by some authors using the Flory–Rehner theory (Ahmad et al., 2015; Chapwanya and Misra, 2015; Nelson et al., 2020; van der Sman, 2015). This mechanism of transporting water to the surface is important since it is estimated that 80% of the water losses during double-sided pan cooking of beef hamburgers is due to drip loss (Oroszvári et al., 2005b; Tornberg, 2013). However, Dhall and Datta (2011) using a poromechanics-based model concluded that evaporation losses exceed drip losses at any time during single-sided contact heating of patties. These contradictory results indicate the importance of cooking conditions in the moisture transport and emphasize the necessity of elucidating the relationship between the mechanisms driving moisture transport, water phase changes, and heat transfer. Some models have incorporated, using Darcy's law, the transfer of moisture in hamburgers due to contraction pressure as a result of the protein denaturation (Dhall et al., 2012; Ou and Mittal, 2006, 2007). However, these models do not explicitly consider the shrinkage of the solid matrix. To the best of our knowledge, with the exception of the works of Dhall and Datta (2011) and Moya et al. (2021), there are no mathematical models that address meat deformation during contact heat transfer.

Taking these considerations into account, a validated mathematical model of hamburger pan cooking has been developed with the objectives of: (i) achieving more efficient cooking by analysing the influence of pan temperature on thermal changes, moisture loss and shrinkage during domestic pan-cooking of beef burgers; (ii) evaluating the contribution to moisture loss of dripping and evaporation phenomena. An experimental setup, based on a domestic induction hob, was developed with sensing devices to obtain data of the above-mentioned variables over time. Additionally, due to its characteristic composition and structure, a gellan gel of identical shape and size to those of the meat samples were used as a food model in which dripping losses could be considered negligible.

2. Mathematical model

The process of pan-frying hamburgers can be considered as a flow and transport problem in a deforming solid matrix during thermal processing. In this study, the mathematical model that describes these phenomena was developed making several assumptions (Moya et al., 2021). First, the hamburger is considered as a porous material comprising of a solid matrix saturated with liquid water. This two-phase material is assumed to be homogeneous and its mechanical behaviour as hyper-elastic. In other words, the relationship between stresses and strains in the domain is nonlinear. During contact heating, the temperature is considered the same for the two phases and the pressure gradient caused by the shrinking connective tissue induces a flow that follows Darcy's law. Additionally to these assumptions, in this paper new hypotheses have been considered. One is related to the volume change of the meat. While previous models assumed that it was integrally equivalent to the moisture loss (Dhall and Datta, 2011; Moya et al., 2021) in this work, as the experimental results suggested, an additional shrinkage of meat protein was considered. Moreover, when liquid water reaches the bottom surface of the hamburger in contact with the pan, it evaporates extracting heat from the system (Fig. 1).

This effect will influence both the temperature of the product and the pan.

To formulate the mathematical model the volume fraction ϕ_α for each phase should be defined:

$$\phi_\alpha = \lim_{V \to 0} \frac{V_\alpha}{V}, \qquad \alpha = s, w \tag{1}$$

where V_α is the volume occupied by the α phase (solid and water) $V = V_s + V_w$ is the total volume and $\phi_s + \phi_w = 1$.

The kinematics of the meat deformation is described following a representation commonly used for the formulation of solids subjected to finite strains (Dhall and Datta, 2011; Moya et al., 2021; Vujosevic and Lubarda, 2002). A series of fictitious states are considered representing different physical changes that derive in a multiplicative decomposition of the strain deformation gradient $\boldsymbol{F}$ (Fig. 2). Assuming that the deformation of the hamburger due to temperature effects is small and therefore can be neglected, the strain deformation gradient can be expressed as the product of the deformation associated with the water volume loss ($\boldsymbol{F}_w$), the protein shrinkage ($\boldsymbol{F}_p$), and the elastic deformation of the solid phase ($\boldsymbol{F}_e$):

$$\boldsymbol{F} = \boldsymbol{F}_w \boldsymbol{F}_p \boldsymbol{F}_e \tag{2}$$

The volume change due to moisture loss, J_M, can be calculated by relating it to the change in the volume fraction, ϕ_w, of the liquid water phase:

$$J_M = \frac{1 - \phi_{w,0}}{1 - \phi_w} \tag{3}$$

The moisture deformation gradient is defined by:

$$\boldsymbol{F}_w = J_M^{1/3} \boldsymbol{I} \tag{4}$$

with $\boldsymbol{I}$ the $[3 \times 3]$ identity matrix and the jacobian raised to the power of $1/3$ to make $\det(\boldsymbol{F}_w) = J_M$.

It has been assumed that during preparation, the minced meat loses the anisotropy associated to the muscle fibers. Therefore, an isotropic deformation gradient associated to the protein shrinkage in the hamburger can be expressed as:

$$\boldsymbol{F}_{p \text{ local}} = \boldsymbol{F}_p = \begin{bmatrix} \lambda(T) & 0 & 0 \\ 0 & \lambda(T) & 0 \\ 0 & 0 & \lambda(T) \end{bmatrix} \tag{5}$$

where $\lambda(T)$ is a shortening stretch that takes into account the protein shrinkage dependence on the temperature and is proposed to be:

$$\lambda(T) = \begin{cases} 1 & T < 30 \,°C \\ (\lambda_s - 1)(0.02T - 0.6) + 1 & 30 \,°C \leq T \leq 80 \,°C \\ \lambda_s & 80 \,°C < T \end{cases} \tag{6}$$

Where λ_s is a parameter representing the maximum protein shrinkage (Fig. 3). Note that between the temperature range from 30 °C to 80 °C, λ shows a linear dependence on the temperature.

When neglecting body forces and inertia effects, conservation of the linear momentum results in the quasi-static equilibrium equation $\nabla \boldsymbol{\sigma} = 0$ for the material, with $\boldsymbol{\sigma}$ the total Cauchy stress. Conservation of the angular momentum yields the symmetry of this stress tensor that can be expressed as the sum of the partial solid stress and the partial fluid stress:

$$\boldsymbol{\sigma} = \hat{\boldsymbol{\sigma}}_s + \hat{\boldsymbol{\sigma}}_w \tag{7}$$

where

$$\hat{\boldsymbol{\sigma}}_s = \phi_s \boldsymbol{\sigma}_e \qquad \text{and} \qquad \hat{\boldsymbol{\sigma}}_w = \phi_w \boldsymbol{\sigma}_w = -\phi_w p_w \boldsymbol{I} \tag{8}$$

where $\boldsymbol{\sigma}_e$ represents the Cauchy elastic stress of the meat and p_w the volume averaged pressure exerted by the liquid water.

A material that can undergo significant deformation even under large loads is referred to as a hyperelastic material. Hyperelastic materials exhibit nonlinear stress–strain behaviour and can undergo large
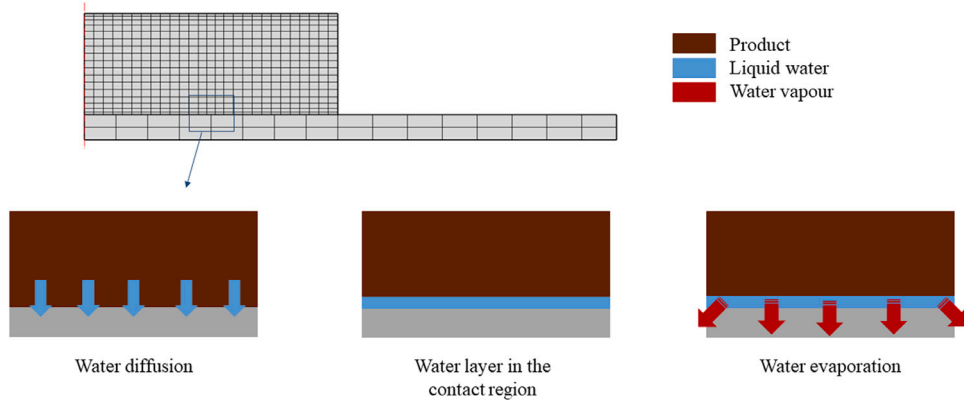
Fig. 1. Schematic representation of the evaporation effect at the contact surface between the food and the pan.
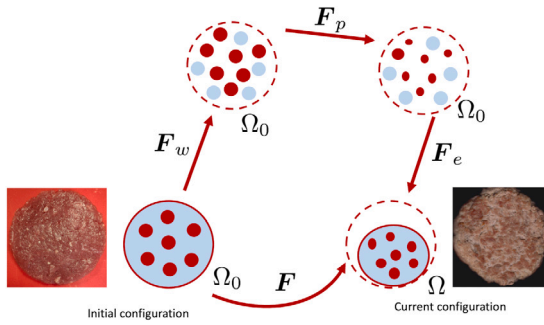

Fig. 2. Schematic representation of the hamburger deformation using two fictitious intermediate steps where protein and water content change along the process. The deformation gradient tensor F is multiplicatively decomposed in three parts associated with the water volume change, F_w, the protein shrinkage, F_p, and the elastic deformation F_e that restores the compatibility such that Ω becomes a compatible configuration.
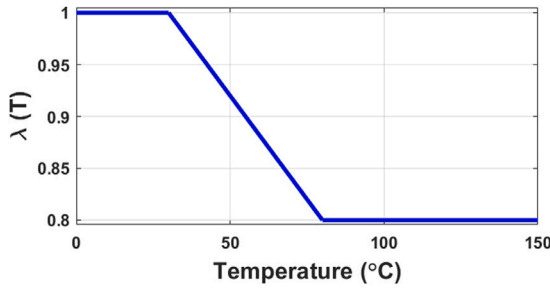

Fig. 3. Evolution of the isotropic shortening stretch $\lambda(T)$ of the meat protein with temperature.

elastic deformations while still being able to return to their original shape once the load is removed. The stress–strain relationship of these materials is derived from a constitutive model. As in a previous study (Moya et al., 2021), the model selected for simulating the hyperelastic behaviour of the meat is based on the isotropic nearly incompressible Neo-Hookean material. The decoupled form of the strain energy function is:

$$\Psi\left(\boldsymbol{C}_e\right) = \Psi_{vol}(J_e) + \bar{\Psi}(\bar{\boldsymbol{C}}_e) = \frac{K}{2}\left(J_e - 1\right)^2 + \frac{G'}{2}\left(\bar{I}_1 - 3\right) \quad (9)$$

where K and G' are the bulk and the shear elastic modulus, $J_e = det(\boldsymbol{F}_e)$ and $\bar{I}_1 = \text{tr}\bar{\boldsymbol{C}}_e$ is the first invariant of the modified (deviatoric) right Cauchy–Green tensor $\bar{\boldsymbol{C}}_e = \bar{\boldsymbol{F}}_e^T\bar{\boldsymbol{F}}_e$, with $\bar{\boldsymbol{F}}_e = J_e^{-1/3}\boldsymbol{F}_e$. For a comprehensive description of continuum mechanics kinematics and hyperelasticity, the reader is referred to Bonet and Wood (2008).

A measure of the stress state of a solid in the undeformed or reference configuration is the second Piola–Kirchhoff stress tensor. Taking a force vector in the current configuration and locating its counterpart in the undeformed configuration (pull-back), this tensor is this fictitious force divided by the corresponding area element in the reference configuration. The advantage of using this second Piola–Kirchhoff stress tensor is that it can be obtained directly as the derivative of the strain energy in a non-dissipative process:

$$\boldsymbol{S}_e = 2\frac{\partial\Psi(\boldsymbol{C}_e)}{\partial\boldsymbol{C}_e} = \boldsymbol{S}_{e,vol} + \bar{\boldsymbol{S}}_e = J_e p \boldsymbol{C}_e^{-1} + J_e^{-\frac{2}{3}}(\mathbb{I} - \frac{1}{3}\boldsymbol{C}_e^{-1} \otimes \boldsymbol{C}_e) : \widetilde{\boldsymbol{S}}_e \quad (10)$$

where $\boldsymbol{S}_{e,vol}$ and $\bar{\boldsymbol{S}}_e$ are the volumetric and deviatoric parts of the second Piola–Kirchhoff stress tensor. The hydrostatic pressure p and the tensor $\widetilde{\boldsymbol{S}}_e$ are defined as:

$$p = \frac{d\Psi_{vol}(J_e)}{dJ_e} \qquad\qquad \widetilde{\boldsymbol{S}}_e = 2\frac{\partial\bar{\Psi}(\bar{\boldsymbol{C}}_e)}{\partial\bar{\boldsymbol{C}}_e} \quad (11)$$

Another stress measure that is commonly used in the finite element formulation is the Cauchy stress tensor. This tensor is also called the true stress because it is a true measure of the force per unit area in the current, deformed, configuration. The Cauchy stress tensor $\boldsymbol{\sigma}_e$ is $1/J_s$ times the push-forward of $\boldsymbol{S}_e$ ($\boldsymbol{\sigma}_e = J_s^{-1}\chi_*(\boldsymbol{S}_e)$). For a Neo-Hookean material model the explicit expression is a function of the invariant $\bar{I}_1$:

$$\boldsymbol{\sigma}_e = p\boldsymbol{I} + \frac{2}{J_e}dev\left[\bar{\boldsymbol{F}}_e\frac{\partial\bar{\Psi}(\bar{\boldsymbol{C}}_e)}{\partial\bar{\boldsymbol{C}}_e}\bar{\boldsymbol{F}}_e^T\right] = p\boldsymbol{I} + \frac{2}{J_s}\left(\frac{\partial\bar{\Psi}}{\partial\bar{I}_1}\bar{\boldsymbol{b}}_e - \frac{1}{3}\frac{\partial\bar{\Psi}}{\partial\bar{I}_1}\bar{I}_1\boldsymbol{I}\right) \quad (12)$$

with $\boldsymbol{I}$ being the second-order identity tensor, $dev(\cdot) = (\cdot) - \frac{1}{3}[(\cdot) : \boldsymbol{I}]\boldsymbol{I}$ and $\bar{\boldsymbol{b}}_e = \bar{\boldsymbol{F}}_e^T\bar{\boldsymbol{F}}_e$ the modified left Cauchy–Green tensor.

The mass conservation equation for liquid water is:

$$\frac{\partial c_w}{\partial t} + \nabla \cdot \boldsymbol{n}_w = 0 \quad (13)$$

where $c_w = \phi_w\rho_w$ is the concentrations of liquid water, and $\boldsymbol{n}_w$ corresponds to the absolute flux of liquid water:

$$\boldsymbol{n}_w = \boldsymbol{n}_{w,G} - D_{wT}\nabla T \quad (14)$$

where D_{wT} is the diffusivity due to the temperature gradient and the net flux of liquid water with respect to the ground frame, $\boldsymbol{n}_{w,G}$, can be described by:

$$\boldsymbol{n}_{w,G} = -D_w\nabla c_w + c_w \cdot \vec{v}_{s,G} \quad (15)$$

where D_w is the diffusivity due to the water gradient concentration and $\vec{v}_{s,G}$ is the solid velocity.

Assuming thermal equilibrium between the two phases, the energy balance equation can be written as (Gulati and Datta, 2015):

$$\rho_{eff}C_{p,eff}\frac{\partial T}{\partial t} + \sum_w\left(\boldsymbol{n}_{w,G} \cdot \nabla(C_{eff,w}T)\right) = \nabla \cdot \left(k_{eff}\nabla T\right) \quad (16)$$

The properties of the product, $\rho_{eff}, C_{p,eff}, k_{eff}$, are obtained as a function of temperature and composition (Choi and Okos, 1986):

$$\rho_{eff}(T) = (1 - \phi_w)\bar{\rho}_s + \phi_w\bar{\rho}_w \tag{17}$$

$$C_{p,eff}(T) = x_s C_{p,s} + x_w C_{p,w} \tag{18}$$

$$k_{eff}(T) = (1 - \phi_w)k_s + \phi_w k_w \tag{19}$$

where x_s is the solid phase mass fraction and x_w is that of water.

For the meat, the density of the solid phase was determined by the mass fractions of the protein x_{prot} and fat x_{fat}. The meat density was calculated as a function of temperature and composition as follows (Nesvadba, 2014):

$$\bar{\rho}_s(T) = \left(\frac{x_{prot}}{\bar{\rho}_{prot}(T)} + \frac{x_{fat}}{\bar{\rho}_{fat}(T)} \right)^{-1} \tag{20}$$

The specific heat of the product $C_{p,s}(T)$ was defined for each component and then calculated using a mass fractions average mixing rule:

$$C_{p,s}(T) = x_{prot} C_{p,prot}(T) + x_{fat} C_{p,fat}(T) \tag{21}$$

Isotropic thermal conductivity is assumed for the product lying between two limiting values. The lower limit is given by a perpendicular model with all the constituents in layers perpendicular to the flow of heat $\frac{1}{k_\perp(T)} = \sum_i \frac{\phi_i}{k_i(T)}$. The upper limit is the parallel model in which the constituents are arranged as parallel layers $k_\parallel(T) = \sum_i \phi_i k_i(T)$). The thermal conductivity of the product combining this two limiting values can be estimated as:

$$k_s(T) = g k_\perp(T) + (1 - g)k_\parallel(T) \tag{22}$$

where g is a parameter between zero and one (Nesvadba, 2014), which for $g = 0.5$ provides the arithmetic mean of the lower and upper thermal conductivity limits.

For the gellan gum gel, only the water properties are considered, i.e. $\phi_w = 1$. For this reason, the effective properties are equal to those for the liquid water.

$$\rho_{eff}(T) = \bar{\rho}_w \qquad C_{p,eff}(T) = C_{p,w} \qquad k_{eff}(T) = k_w \tag{23}$$

A series of boundary conditions for the different problem physics should be considered in the model. The contact heat transfer between the pan and the burger can be written as:

$$- k_{pan} \frac{\partial T}{\partial z}\Big|_{z_{pan}=0} = -k_p \frac{\partial T}{\partial z}\Big|_{z_{meat}=0} = H_c (T_{pan} - T_{surf}) \tag{24}$$

where T_{pan} and T_{surf} are the temperatures of the pan and the meat on the contact surface, and k_{pan} and k_p are the thermal conductivity of the pan and the product, respectively. The parameter H_c refers to the thermal conductance between both surfaces and plays an important role in the model since it regulates the heat flow received by the product. As will be shown below, in the contact region a boundary layer of water and vapour quickly forms when the product is added. Since this layer remains throughout the entire cooking process, this parameter has been assumed as constant.

To obtain the energy absorbed by water during the evaporation process in this contact region, an expression for q_{evap} based on that proposed by Feyissa et al. (2011) was used to incorporate this boundary condition:

$$q_{evap} = \sigma_{evap} \bar{\rho}_w L_{evap} e f_v(T_{surf}) \tag{25}$$

where σ_{evap} is the evaporation rate constant, L_{evap} is the water latent heat of vaporization, e is the thickness of the liquid water layer and f_v is a sigmoid function given by:

$$f_v = \frac{1}{1 + e^{0.107(-T_{surf}+121)}} \tag{26}$$

A convective heat transfer mechanism was applied in the rest of the surfaces of the product and the pan:

$$q_{surf} = h(T_{amb} - T_{surf}) \tag{27}$$

being h the thermal convection coefficient and T_{amb} the temperature of the surrounding air.

When the temperature increases inside the product, the capacity to retain water decreases causing the dripping phenomena (Hughes et al., 2014). Therefore, the liquid water under the effect of gravity comes into contact with the pan and suddenly evaporates. To account for this effect, the model considered the dripping phenomena at the lateral boundary as:

$$n_{w,surf} = \mathbf{n}_w \cdot \mathbf{N}_{surf} \tag{28}$$

where $\mathbf{n}_w$ is the absolute flux of liquid water described in Eq. (14) and $\mathbf{N}_{surf}$ is the normal vector to the surface.

The commercially available finite element software, COMSOL Multiphysics 5.3a software, was used to implement the equations of the mathematical model.

3. Materials and methods

3.1. Gellan gum gel sample preparation

A gellan gum gel was prepared with the following composition: 98.3% (w/w) tap water (210–240 mg/L $CaCO_3$), 1.2% (w/w) deacylated gellan gum powder (Texturas, Albert and Ferran Adrià, Bidfood Iberia, Barcelona), and 0.5% (w/w) calcium chloride dihydrate (Sigma Aldrich, Darmstadt, Germany). The gelling agent was dispersed in the water using an electric blender. After hydration of the gellan gum, the mixture was brought to the boil. The calcium salt was added and stirring was continued until it was dispersed. The mixture was then poured onto a tray and refrigerated at 4 °C for 24 h. Using a mould, cylinders similar in size to hamburgers (100 mm in diameter and 20 mm in height) were extracted. Pieces 2 mm thick (2 g) were removed with a meat slicer to determine the water retention capacity and 4 mm thick (50 mm in diameter) for rheological analysis.

3.2. Beef hamburger preparation

Patties were made from the middle part of beef loin (*Longissimus dorsi* muscle). The meat was ground through a 3 mm grinder plate. A manual 100 mm diameter hamburger press was used to shape the meat in cylindrical pieces of 180 g (20 mm thick) in weight. Small patties of 9 g with a thickness of 4 mm and a diameter of 50 mm were also prepared for the determination of water retention capacity and rheological properties.

3.3. Water holding capacity

The ability of the meat to resist the removal of water was determined in the same manner as described in Moya et al. (2021) following the method of Goñi and Salvadori (2010). Small patties of minced meat were placed inside open plastic bags and subjected to heat treatments by immersion in a water bath at controlled temperature (Digiterm S–150, JP Selecta, Abrera, Spain), from 30 °C to 100 °C, for 30 min and then rapidly cooled in an ice-water bath. Small pieces of the gellan gum gel were placed in a thermostatic oven, since if the determination was carried out in a thermostatic bath, as in the case of the meat, the gel would reabsorb the released water. The final moisture content of the products, considered as the water holding capacity (WHC), was determined by weight the difference after drying in a convection oven at 105 °C for 24 h (AOAC, 2002) and expressed as kg water/kg dry material. Ten replicas were carried out for each temperature and product.
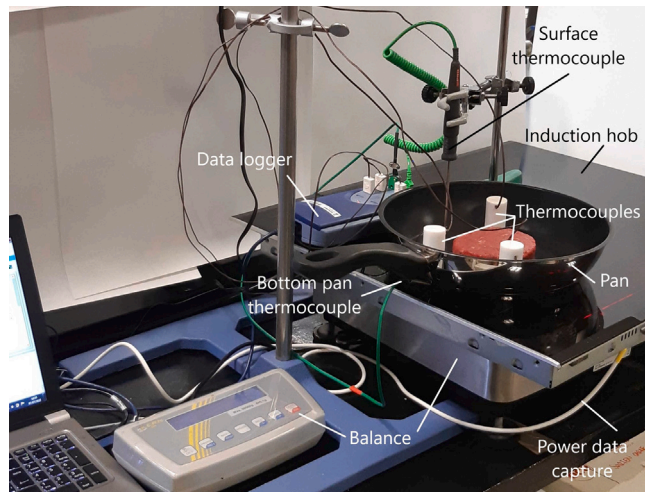
Fig. 4. Experimental setup for temperature and weight loss measurement during the cooking process.

3.4. Rheological measurement

The rheological properties of the minced meat and the gel were measured as described in Moya et al. (2021) using a Physica MRC 301 rheometer (Anton Paar GmbH, Graz, Austria), equipped with serrated parallel plate geometry (50 mm, 4 mm gap) and a temperature controller ($\pm 0.5°C$). Frequency and stress sweeps (from 0.1 to 10 Hz and from 0.1 to 1000 Pa) were performed to determine the linear viscoelastic region. In this way, it was established that the dynamic oscillating tests were executed at a frequency of 2 Hz and a stress of 3 Pa. The evolution of the storage and loss modulus was determined from the data obtained from five replicates of each product, in increasing temperature tests from 25 °C to 100 °C, with steps of 5 °C, and residence times of 3 min at each temperature.

3.5. Cooking procedure

Hamburgers and gels were individually cooked in a multilayer pan (0.6 mm of steel at the bottom, 3.5 mm of aluminium in the middle, and 0.8 mm of steel) with a Teflon platinum non-stick coating of 210 mm in diameter (WMF, WMF Group GmbH, Geislingen a der Steige, Germany), heated by an induction hob provided with an automatic temperature control system called "frying sensor" (BOSCH PXY675DW4E/01 model, BSH, Munich, Germany). Fig. 4 shows the experimental setup. Cooking was done at two pan temperatures (140 °C and 215 °C) using the frying sensor at level 2 (F2) and 5 (F5). The products were added to the pan when the pan temperature measured by a surface K type RS PRO thermocouple (RS, London, UK) indicated that a stable temperature of the pan was reached. This was considered to occur when the temperature varied ± 3 °C from the set point (approximately 110 s after turning on the hob). The central bottom pan temperature was also measured by a K type 1.5 mm-diameter thermocouple located in a hole made for this purpose. The products were cooked on one side for 660 s.

The appearance of the hamburgers and the gels during and at the end of cooking is shown in Fig. 5, clearly showing the moisture loss by dripping in the hamburger and the absence of this phenomenon in the gel. The power supplied by the system control of the induction hob to maintain the target temperature was monitored with LabTech software v6.0.1.5 (ConnectWise, Tampa, FL, USA). The evolution of the temperature in different positions inside the products was measured by penetration T type 1.5 mm-diameter thermocouples placed at 2 and 10 mm from the lower surface. All thermocouples were connected to a

data logger (TC-08 Series, Farnell Components, Barcelona, Spain). The average temperature on the upper face of the products was determined from images taken every minute with an infrared thermal camera (875–2 model, Testo, Lenzkirch, Germany). The weight of the products was measured every five seconds with a precision of 0.1 g by a balance (DS30K0.1 L, Kern & Sohn, Balinger-Frommern, Germany) on which the induction hob was located. Each experiment was replicated five times.

3.6. Shrinkage

Pictures of the hamburgers and gels were taken every minute with a mobile phone (Samsung Galaxy A8) placed parallel to the pan. Shrinkage was quantified as the reduction in the surface area of the products. The digital analysis of images taken during the cooking has allowed their determination using the public domain ImageJ software.

3.7. Moisture content

After cooking, samples of 20 mm diameter were removed with a cylindrical punch from the hamburgers and gels. Each of these samples was divided into three sections: a lower one (2 mm high), an upper one (3 mm high), and a central one. The meat and gel sections (five replicates) were analysed for moisture content following the AOAC Method 950.46 (AOAC, 2002).

4. Finite element model

A 2D axisymmetric model was developed to reproduce the cooking process. The geometry of both the aluminium pan with a diameter of 210 mm and 5 mm thickness and the product (gel or beef meat) with a diameter of 100 mm and 20 mm thickness was considered.

The model was meshed with rectangular elements using quadratic approximation for mass transfer, temperature and deformation. A mesh sensitivity analysis was carried out to establish the optimum mesh size. The number of nodes and elements for the model was 504 and 459 elements, respectively (see Fig. 1).

An initial temperature condition of 25 °C on the surface of the pan and a uniform temperature for the burger of 23.4 °C were set. To simulate the experimental procedure, a power control was implemented in the model in order to regulate the heat power required to increase the temperature of the pan.

$$\text{Power} = \begin{cases} K(T^o_{pan} - T^*_{pan}) & \text{if} \quad (T^o_{pan} - T^*_{pan}) < W_{max}/K \\ W_{max} & \text{if} \quad (T^o_{pan} - T^*_{pan}) \geq W_{max}/K \end{cases} \quad (29)$$

where K is a parameter, T^o_{pan} is the objective cooking temperature, T^*_{pan} is the temperature of the bottom surface of the pan and W_{max} is the maximum power applied by the induction hob. In the experiment, this temperature was measured with a Surface Thermocouple, see Fig. 4.

5. Results and discussion

First of all, the results of the product parameters (hamburger and gel) obtained by experimentation and necessary for the development of the model are explained in the following section. The fitting of the model for the two products is then shown by comparing the temperature, water loss and shrinkage. Finally, some results and considerations about the effect of the energy expenditure on the quality of the product are presented.
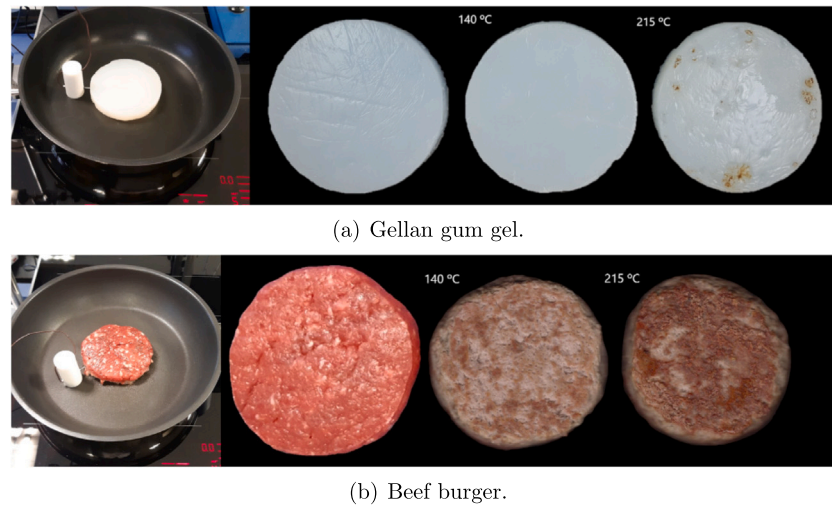
(a) Gellan gum gel.

(b) Beef burger.

Fig. 5. Bottom surface aspect at the beginning and end of the cooking for two different products and two cooking temperature levels, 140 °C (F2) and 215 °C (F5).

5.1. Effect of heating on product properties

5.1.1. Water holding capacity

The impact of temperature on the WHC is depicted in Figs. 6.a and 6.b As anticipated, the WHC of the minced beef decreases with rising temperature due to the thermal denaturation of proteins during cooking, which leads to a reduction in the meat's ability to retain water. The mechanisms underlying sarcomere shortening, which are intricate and continue to be a subject of discussion (Ertbjerg and Puolanne, 2017), are widely recognized to significantly influence the WHC. The relationship between WHC and temperature follows a sigmoidal pattern, consistent with previous findings documented by Dhall and Datta (2011), Goñi and Salvadori (2010), van der Sman (2007) and Kondjoyan et al. (2013). The experimental WHC values align closely with those reported by Moya et al. (2021) for pieces of whole beef and are in agreement with those obtained by Tornberg (2005) according to which the water loss of the burgers was almost as large as for the whole meat. The following function was fitted to the experimental data for the minced meat and gellan gum gel:

$$\text{WHC}_i(T) = c_i - \frac{a_{i1}}{1 + a_{i2}\, exp\left(-a_{i3}\left(T - T_i\right)\right)} \qquad i = m, g \tag{30}$$

where, for the minced meat (from 30 °C to 100 °C) those parameters are: $c_m = 1.537$ kg water/kg dry meat, $a_{m1} = -1.276$ kg water/kg dry meat, $a_{m2} = 0.009818$, $a_{m3} = 0.08349$ °C^{-1} and $T_m = -0.2618$ °C, estimated by a non-linear regression using the Levenberg–Marquardt method ($R^2 = 0.9983$). For the gum gellan gel (from 30 °C to 80 °C) the parameters are $c_g = -102$ kg water/kg dry product, $a_{g1} = -342.6$ kg water/kg dry product, $a_{g2} = 1.076$, $a_{g3} = 0.009564$ °C^{-1} and $T_g = -1.148$ °C ($R^2 = 0.9928$).

In this way, the equilibrium water concentration is related to the WHC through the equation:

$$\rho_w(T) = \text{WHC}_i(T)\rho_s(T) \qquad i = m, g \tag{31}$$

5.1.2. Rheological properties

To assess the temperature dependence of the storage modulus, G', and the phase angle, α, a dynamic temperature sweep ranging from 25 °C to 100 °C was performed (Figs. 6.c and 6.d). For the gellan gum gel, G' shows minimal changes until 45 °C, decreasing thereafter due to the temperature's impact on the strength of network structure connections. The pronounced elastic nature of the gel compared to the viscous component is evident in the phase angle, which remains around 2° until 55 °C, slightly increasing at higher temperatures. This behaviour is consistent with that described by other authors (Fan et al.,

2022; Morris et al., 2012), although the values depend on various factors such as the acyl group content, concentration and type of cations, and pH, among others. For the minced meat, G' exhibits a slight decrease until it reaches a minimum value at 55 °C. However, it experiences a significant increase between 60 °C and 80 °C, possibly due to contraction of the connective tissue, followed by a decrease at temperatures above 80 °C. Throughout the tested temperature range, the phase angle diminishes with a more pronounced decrease observed between 50 °C and 60 °C. These results are similar to those found by Moya et al. (2021) for whole beef loin meat and exhibit the same trend as described by (Tornberg, 2005), although in this case the values differ due to this being another muscle (*M. biceps femoris*).

The gellan gel gum storage modulus, for temperatures between 25 °C and 100 °C, can be defined by Eq. (32):

$$G'(T)_g = G_{a,g} - \frac{G_{b,g}}{1 + G_{c,g} \exp\left(G_{d,g}(T - G_{e,g})\right)} \tag{32}$$

where $G_{a,g} = 57.03$ kPa, $G_{b,g} = 55.14$ kPa, $G_{c,g} = 26.31$, $G_{d,g} = -0.07211$ °C^{-1} and $G_{e,G} = 34.51$ °C, values obtained by adjusting the experimental results obtaining a R^2 of 0.9993. Fig. 6.c shows the experimental value of the storage modulus and its fitting.

The beef burger storage modulus, for temperatures between 25 °C and 100 °C, can be defined by a piecewise Eq. (33):

$$G'(T)_b = \begin{cases} G_{a,b} \cdot T^3 + G_{b,b} \cdot T^2 + G_{c,b} \cdot T + G_{d,b} & \text{if} \quad 25 \text{ °C} \le T < 55 \text{ °C} \\ G_{e,b} + \dfrac{G_{f,b}}{1 + G_{g,b} \exp(G_{h,b}(T - G_{i,b}))} & \text{if} \quad 55 \text{ °C} \le T < 80 \text{ °C} \\ G_{j,b} \cdot T + G_{k,b} & \text{if} \quad 80 \text{ °C} \le T < 100 \text{ °C} \end{cases} \tag{33}$$

where $G_{a,b} = 0.0007341$ kPa °C^{-3}, $G_{b,b} = -0.07776$ kPa °C^{-2}, $G_{c,b} = 2.335$ kPa °C^{-1}, $G_{d,b} = 3.466$ kPa, $G_{e,b} = 42.35$ kPa, $G_{f,b} = 25.62$ kPa, $G_{g,b} = 0.838$, $G_{h,b} = 0.2492$ °C^{-1}, $G_{i,b} = 65.91$ °C, $G_{j,b} = -0.4494$ kPa °C^{-1} and $G_{k,b} = 77.3$ kPa, values obtained by adjusting the experimental results obtaining a R^2 of 0.9998. Fig. 6.d shows the experimental value of the storage modulus and its fitting.

### 5.2. Evolution of temperature, weight loss and shrinkage during cooking

Selecting the power level F2, which implies a pan objective temperature of 140 °C, an iterative process was conducted to find the input parameters of the model that best fit the experimental results. Several Monte Carlo simulations were conducted, randomly varying the input parameters within intervals that were reduced after each round until the final values were found. Table 1 shows the model input parameters,
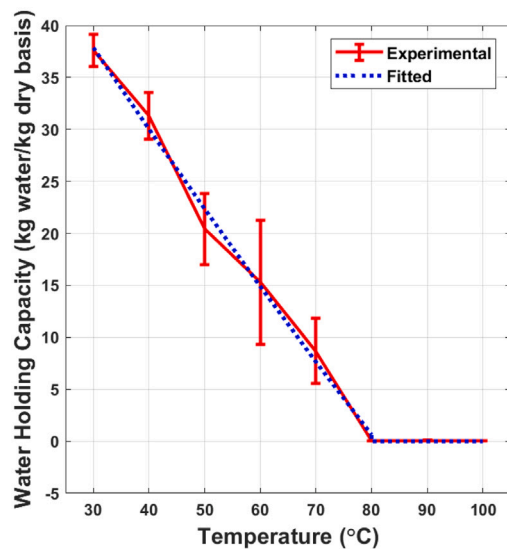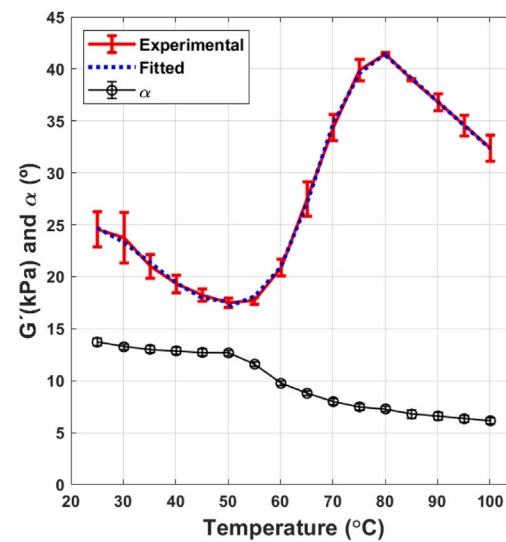
(a) Gellan gum gel
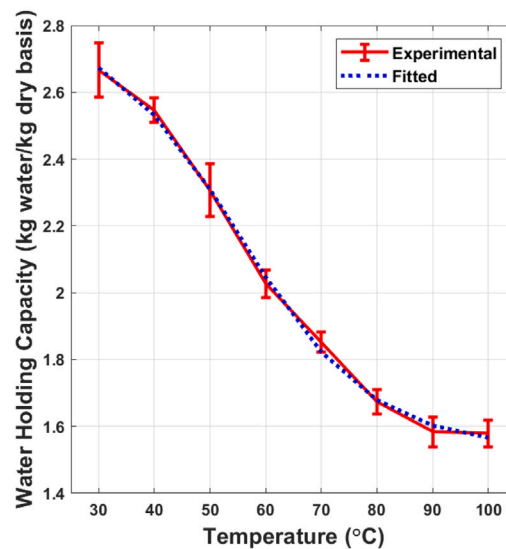
(b) Minced meat
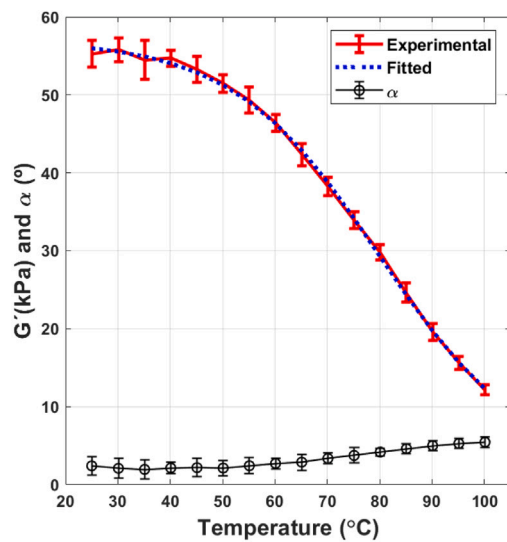
(c) Gellan gum gel

(d) Minced meat

Fig. 6. Water Holding Capacity as a function of temperature T for: (a) Gellan gum gel; (b) Minced meat. Storage modulus, G' (kPa), and phase angle, α (°) as a function of cooking temperature for: (c) Gellan gum gel; (d) Minced meat. Experimental values indicated by symbols and estimated values by the blue line.

indicating those obtained by fitting. After parameter fitting for power level F2, the model was used to predict the experimental results of power level F5. As will be shown in the following sections for both the fitted and predicted results, the model performs with a high degree of accuracy. However, due to the large number of input parameters used, there is a potential risk of overfitting, which should be tested under new cooking conditions.

5.2.1. Temperature

Fig. 7 shows the temperature evolution during cooking at the central point of the product and at 2 mm above the bottom surface, and the average temperature of the upper surface for both the gellan gum gel and beef burger for the two power levels (F2 and F5). The results indicate that in both products, the temperature of the pan hardly influences the temperature evolution at the central point (65.5 and 63.6 °C for the gel, and 67.7 and 68.9 °C for the burger at F2 and F5, respectively,

at t=660 s). This can be explained because these products are mostly composed of water, which absorbs a significant amount of heat when it evaporates. As a result, three zones can be distinguished throughout the thickness. The first corresponds to a dehydrated region on the lower side in contact with the pan, where the temperature increases rapidly but progresses slowly towards the interior because a substantial amount of heat is required to evaporate the water reaching it (Fig. 1). In the case of the meat, it is in this zone where the Maillard reaction takes place at a sufficient speed to generate the characteristic aromatic compounds and brown colour. There is a second boiling region where the temperature does not exceed 100 °C, even when cooking at high power levels, as indicated by experimental data at 2 mm from the lower side. Finally, there is a third zone where the heat is transmitted through conduction to the upper layers with a constant driving force (Myhrvold et al., 2011). Consequently, regardless of the selected power level, the time required to reach the desired central temperature will be

Table 1
Model input parameters.

Name and description	Value	Source
Model parameters		
K controller parameter [W/°C]	84	Fitted
W_{max} Maximum induction hob power [W]	2200	Measured
T_{amb} surrounding air temperature [°C]	25	Measured
T_{pan}^o pan objective temperature [°C]	140 or 210	Measured
P_{amb} environment pressure [kPa]	$1.01 \cdot 10^2$	Measured
H_c thermal conductance of pan-meat contact [W/(m² K)]	200	Fitted
g thermal conductivity parameter	0	Fitted
h convection coefficient [W/(m² K)]	5	Fitted
Water properties		
$\overline{\rho}_w$ water density [kg/m³]	997.2	Choi and Okos (1986)
D_w water diffusivity [m²/s]	$2.104 \cdot 10^{-9}$	Fitted
$D_{w,T}$ water diffusivity due to temperature gradient [kg/(m s K)]	$D_w \cdot \frac{\partial \rho_{f,eq}}{\partial T}$	Fitted
$C_{p,w}$ water specific heat [kJ/(kg °C)]	$4.129 - 9.09 \cdot 10^{-5} \cdot T$ $+5.473 \cdot 10^{-6} \cdot T^2$	Choi and Okos (1986)
k_w water thermal conductivity [W/(m K)]	0.57	Choi and Okos (1986)
L_{evap} vaporization latent heat [J/kg]	$2.26 \cdot 10^6$	Straub (1985)
h_m mass transfer coefficient [m/s]	$1.688 \cdot 10^{-3}$	Fitted
σ_{evap} evaporation ratio [1/s]	$1.604 \cdot 10^{-3}$	Fitted
Meat properties		
$\overline{\rho}_p$ meat density [kg/m³]	1330	Choi and Okos (1986)
$C_{p,s}$ meat specific heat [J/(kg K)]	$2.008 + 1.209 \cdot 10^{-3} \cdot T$ $-1.313 \cdot 10^{-6} \cdot T^2$	Choi and Okos (1986)
k_p product thermal conductivity [W/(m K)]	$1.788 \cdot 10^{-1} + 1.196 \cdot (10^{-3}) \cdot T$ $-2.718 \cdot (10^{-6}) \cdot T^2$	Choi and Okos (1986)
WHC water holding capacity [kg water/kg dry material]	Fig. 6b.	Measured
G' storage modulus [kPa]	Fig. 6d.	Measured
λ_r shrinkage effect parameter	0.8	Fitted
Gellan gum gel properties		
WHC water holding capacity [kg water/kg dry material]	Fig. 6a.	Measured
G' storage modulus [kPa]	Fig. 6c.	Measured

practically the same. The upper surface reaches a temperature between 3–4 °C higher when cooked with F5 compared to F2, possibly due to the convective heat transfer from the surrounding air near the pan. These results differ from those obtained by Oroszvári et al. (2005a) and Pan et al. (2000) because according to these authors, the higher the heating temperature, the shorter the total cooking time to reach the same internal temperature. This discrepancy may be because the burgers, in the aforementioned studies, were cooked frozen, and the higher temperature of the plates resulted in shorter thawing times at the center of the burgers. However, unlike what occurs in the work of Pan et al. (2000), in the study by Oroszvári et al. (2005a) temperatures near the surface do not exceed 100 °C. Another noteworthy aspect is that the temperature evolution in the gel is similar to that of the burger, reaching very similar temperatures at the end of the cooking time. The different composition of the meat and the gel does not sufficiently affect the parameters related to heat transfer (specific heat and thermal conductivity) to be a decisive factor in the thermal evolution of both products.

The temperatures predicted by the model are also shown in Fig. 7. The computational calculations have taken into account the uncertainty in the thermocouple position (estimated at ±1 mm), considering possible sensor displacements as computational digressions. The Root Mean Squared Error (RMSE) was calculated between the predicted and experimental values. The RMSE obtained for the central temperature in the gellan gum gel was 1.32 °C for both power levels. For the beef burger, the RMSE values were 2.72 and 4.02 °C for F2 and F5, respectively. For the temperature at 2 mm above the bottom surface, the RMSE values were more pronounced (for the gel: 4.98 °C at F2 and 2.49 °C at F5; for the burger: 3.30 °C at F2 and 11.45 °C at F5). This could be due to the significant temperature differences within a very thin layer of the product. For the top surface, the errors for the gel

were 3.11 and 3.59 °C at F2 and F5, respectively, increasing to 7.96 and 6.34 °C in the case of beef burger. These errors may be a consequence of assuming a constant temperature of the surrounding air during the cooking.

5.2.2. Weight loss

The weight loss of the gellan gum gel and the burger follows a linear trend over time for both power levels (Fig. 8). However, despite having almost the same temperature distribution, there is a significant difference in the amount of weight lost during cooking. At the end of the cooking process, the gel experiences a weight loss of 9.62% and 16.72%, while the burger loses 4.40% and 12.23% at power levels F2 and F5, respectively. The higher heat input results in more vapour generation, but the fact that evaporation limits the temperature to 100 °C causes the boiling region to act as a thermal resistance to heat transmission. As expected, considering the water retention capacity of the two products (Fig. 6a and b), the gel loses a greater amount of water compared to the burger under the same conditions. The protein structure of the meat has a better ability to retain water compared to the coaxial double helix structure of gellan gum (Morris et al., 2012). The developed model is capable of accurately predicting these weight losses with RMSE values of 0.76% and 1.20% for the gel, and 0.57% and 0.98% for the burger at power levels F2 and F5, respectively.

The distribution of humidity and temperature inside the hamburger according to the model predictions is shown in Fig. 9. It can be visually observed that there is a similarity in the temperature distribution for the two power levels at the end and halfway through cooking. However, the same cannot be said for humidity. The hamburger cooked at F5 has experienced greater dehydration in the region close to the pan compared to the one cooked at the lower power. These predictions align with the experimental data, as a humidity of 61.76±3.46 % was obtained
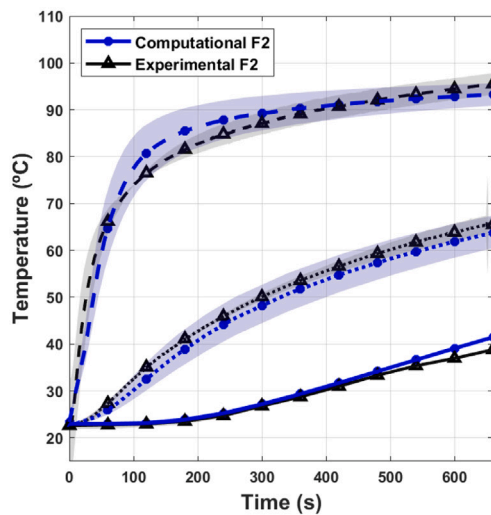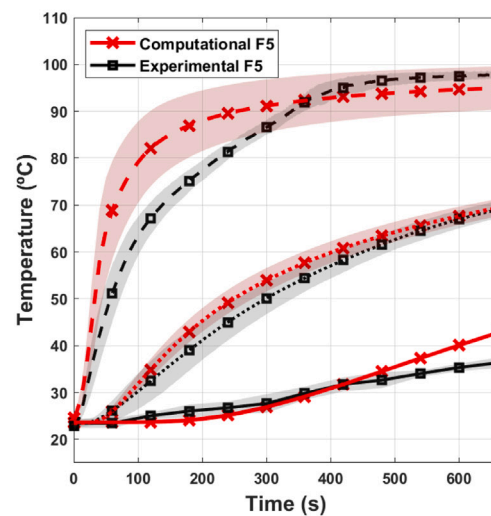
(a) Gellan gum gel cooked at F2
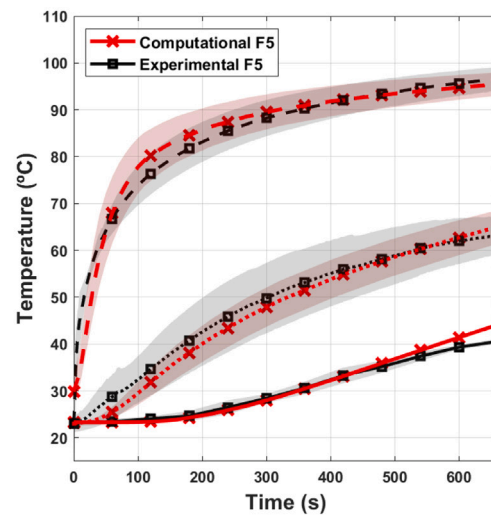
(b) Gellan gum gel cooked at F5
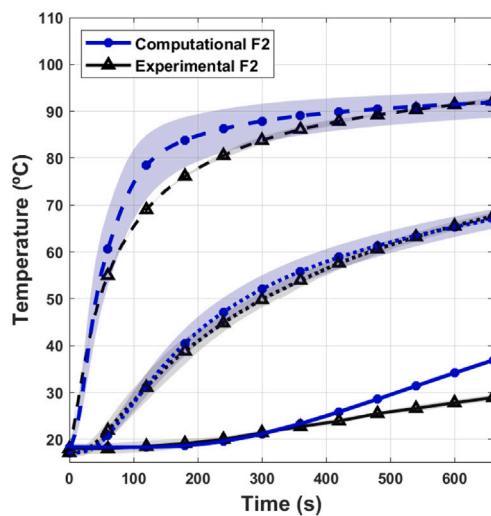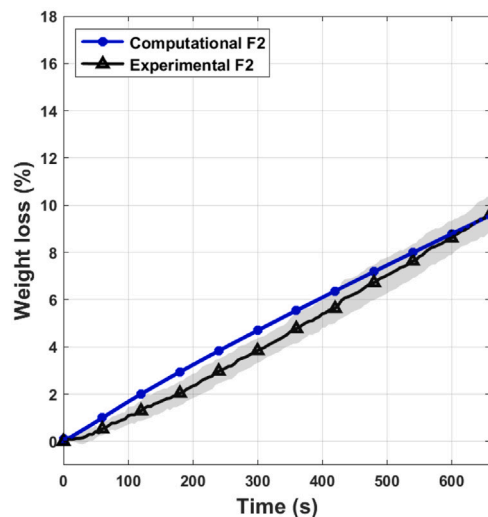

(c) Burger cooked at F2

(d) Burger cooked at F5

Fig. 7. Evolution of temperature in the products cooked at two power levels (F2 and F5): (a) and (b) for gellan gum gel and (c) and (d) for beef burger. The upper surface mean temperature shown by the solid line, the temperature at 2 mm above the bottom surface by the dashed line and the temperature at the central point by the dotted line.

in the lower zone, 72.39 ± 0.33 % in the central zone, and 76.73 ± 0.16 % in the upper zone at F5, while at F2 these values were 68.49 ± 0.62, 72.78 ± 0.84, and 75.72 ± 1.36 % for the lower, central, and upper zones, respectively. A similar behaviour was observed in the gels, where the humidity in the lower zone was 96.97 ± 0.14 % and 97.79 ± 0.17 % for F5 and F2, respectively, and was practically the same as the initial humidity in the central and upper zones.

5.2.3. Shrinkage

During heating, the thermal denaturation of myosin and actin and the helix-to coil transition of collagen promotes the collapse of the protein network and causes structural changes such as transversal and longitudinal shrinkage of muscle fibers. These changes alter the water holding capacity, and the water is expelled due to the pressure exerted by shrinking tissues on the aqueous solution in the extracellular void (Tornberg, 2005). The developed model takes these phenomena

into account in the computation of water transport and in the prediction of product deformation. Fig. 10 shows the evolution of the upper area of the burger during cooking for the two power levels predicted by the model, along with data experimentally obtained from digital image analysis. At the end of cooking, the surface retraction is 6.4% and 10.6% for F2 and F5, respectively. These differences between the two power levels were expected considering the evolution of weight loss. The model adequately reproduces the retraction with an RMSE of 0.71% and 0.60% for F2 and F5, respectively. Shrinkage in meat has been determined in different ways: as a change in superficial area through video image analysis (Barbera and Tassone, 2006) or as a change in average diameter, short and long axes, perimeter, volume and surface area using 3D laser scanning (Vaskoska et al., 2020) or image analysis (Du and Nekovei, 2005; Zheng et al., 2007). In the case of burgers, retraction has occasionally been estimated by changes in diameter (Pan and Singh, 2001; Dhall and Datta, 2011; Oroszvári et al., 2005a,b, 2006). However, these same authors note that the
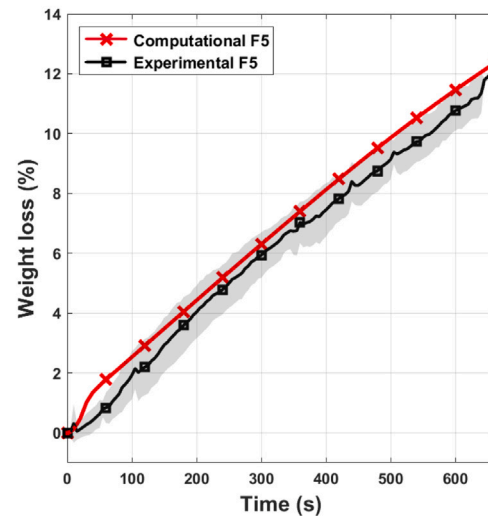
(a) Gellan gum gel cooked at F2
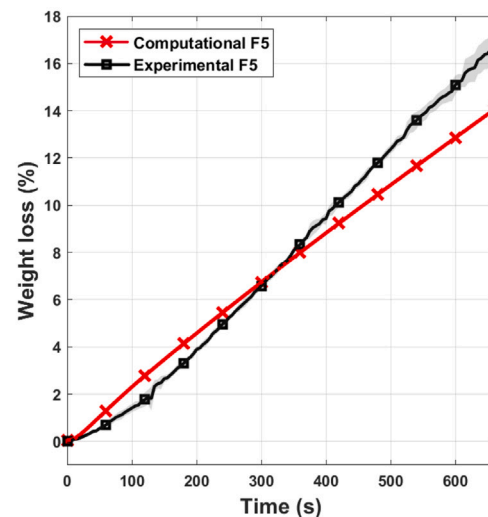
(b) Gellan gum gel cooked at F5
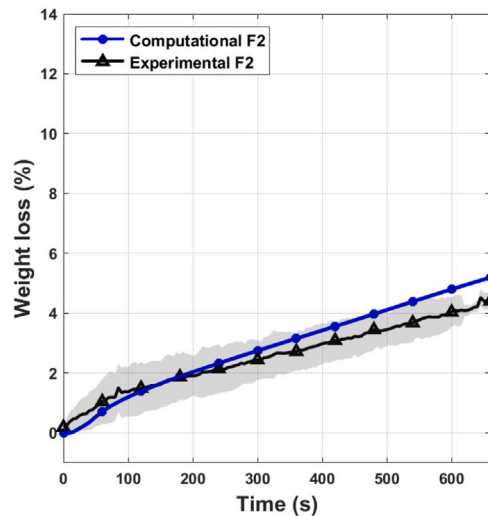
(c) Beef burger cooked at F2

(d) Beef burger cooked at F5

Fig. 8. Water loss evolution in products cooked at the two power levels (F2 and F5): (a) and (b) for gellan gum gel, and (c) and (d) for beef burger.

diameter takes different values depending on the height at which it is measured, indicating non-uniformity in burger shrinkage. Thickness is another parameter used to quantify changes in patty dimensions during cooking, having been found to increase up to a maximum and then decrease slightly (Pan and Singh, 2001). In this work, thickness was not used to evaluate the deformation of the patties because it was very difficult to quantify correctly. The thickness of the patty at the end of cooking measured with a caliper was not uniform in all radial positions, presenting a greater increase in the center of the patties than at the edges. This behaviour has been described previously (Dagerskog, 1979). Experimentally, the values of shrinkage do not exactly match those of weight loss (see Figs. 8 and 10) and the proposed model that considers the multiplicative decomposition of the strain deformation gradient is capable of predicting this behaviour. In some studies (Barbera and Tassone, 2006), differences have also been found between the values of weight loss and shrinkage determined as changes in the upper area of meat cylinders, suggesting that shrinkage provides specific and

complementary information to weight loss and that they can be used together to estimate the changes that occur during the cooking of meat.

The model does not consider shrinkage effects in gellan gum since the upper area only reduces by 0.752% and 1.217% for power levels F2 and F5, respectively. This indicates that the weight loss of this product is almost exclusively due to water evaporation upon contact with the pan. The loss of water through dripping occurring in meat, caused by the mechanical force exerted by protein retraction, is practically negligible in gellam gum. These differences between both products were visually observed during the cooking process (see Fig. 5). Fig. 11 compares the contribution of evaporation and dripping to water loss during gellan gum gel and beef burger cooking predicted by the model. While the gel model does not show any loss through dripping, burger dripping loss reaches 21.5% (F2) and 14.3% (F5) of the total water loss. The contribution to water loss through dripping with F5 is similar to that obtained by Dhall and Datta (2011) in single-sided cooked patties at 140 °C.
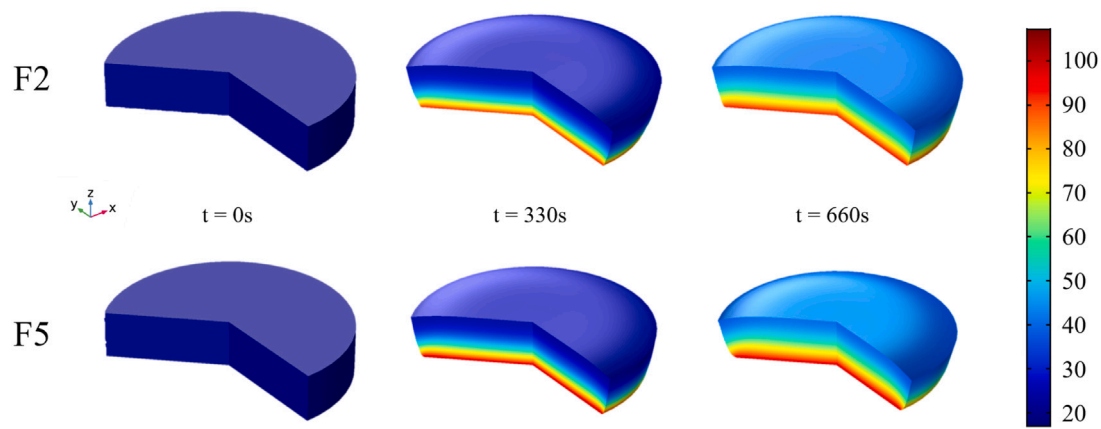
(a) Temperature distribution
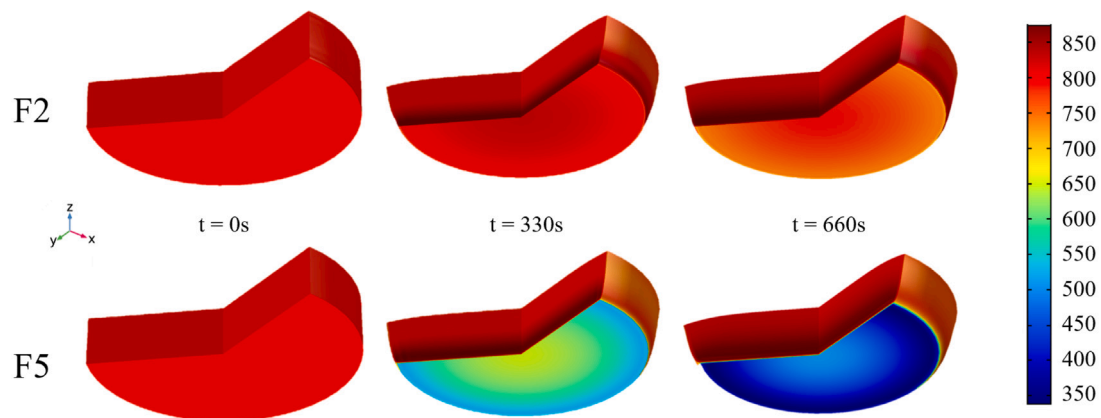
(b) Water concentration distribution

Fig. 9. Distribution of temperature (°C) and water concentration (kg/m^3) in the burger at different cooking times for two power levels (F2 and F5).

5.3. Energy consumption versus quality

In the meat cooking process, a balance between efficiency and product quality is considered because attempting to cook with the lowest possible energy consumption can compromise certain attributes such as tenderness or juiciness. Based on the temperature evolution at different points of the burger and the weight loss, it has been observed that an increase in energy transmitted by the inductor when increasing the power level does not result in a faster heating front progress. Therefore, the time to reach the desired temperature in the center of the product, depending on the desired degree of doneness, remains the same regardless of the selected power level. Hence, in this type of cooking, lower energy consumption entails cooking at a lower power level.

According to the computational results, during cooking the gellan gum gel, the amount of energy absorbed without considering that used in the evaporation process at power level F2 was 26.46 kJ and 29.15 kJ at F5. The energy supplied by the inductor was 170.62 kJ and 317.28

kJ, respectively. The results for the meat burger showed an absorbed energy of 26.93 kJ at F2 and 31.53 kJ at F5 under the same condition. However, it required 152.19 kJ and 259.72 kJ of energy to reach the target temperature for F2 and F5, respectively. These data indicate that energy consumption is not only higher with a higher power level but that there is also greater water loss during cooking since to maintain the pan at the desired temperature, the heat removed in the form of latent evaporation must be replenished.

It seems that cooking at a low power level would not adversely affect product quality in terms of juiciness, as hamburgers cooked this way retain a higher amount of water. At both power levels, F2 and F5, the temperature (T ≥ 140 °C) is sufficiently high for the Maillard reaction to be triggered in the region of the burger close to the surface of the pan, resulting in the generation of compounds that give the characteristic taste, flavour, and colour to grilled meat Nursten (2005). However, the intensity of the flavour may differ under both conditions, which would need to be elucidated through sensory analysis or analysis of odour-active volatile compounds (Sohail et al., 2022).
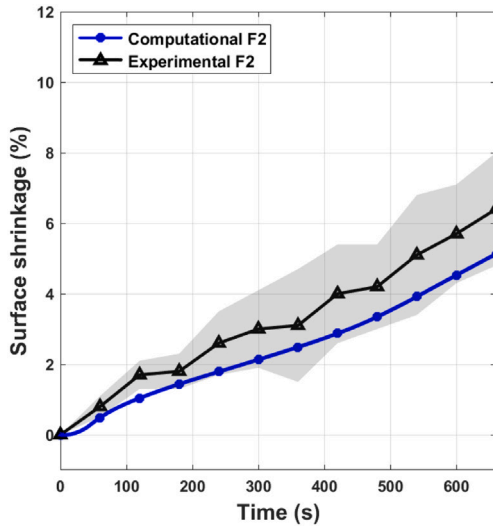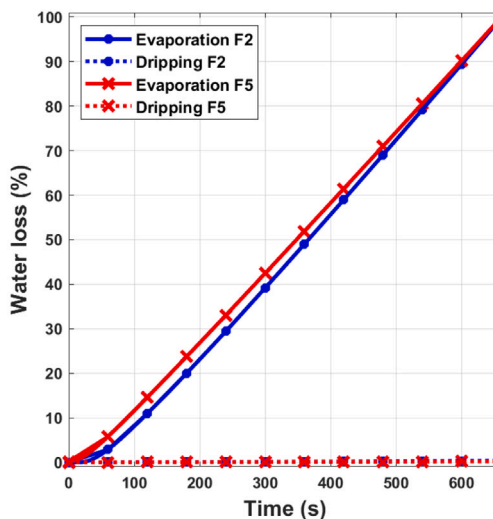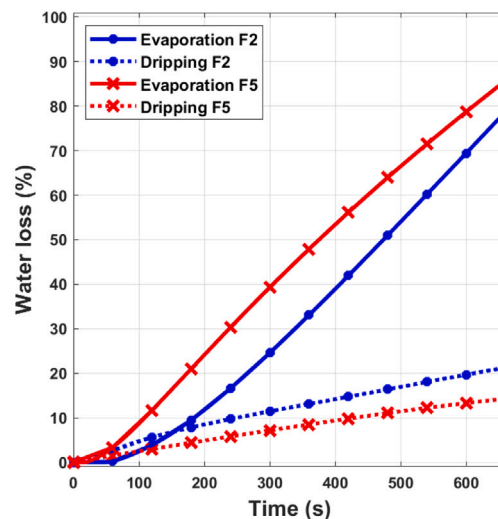
(a) Burger cooked at F2
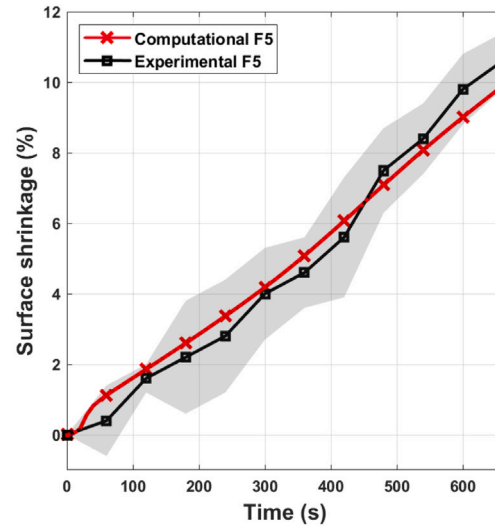
(b) Burger cooked at F5

Fig. 10. Beef burger shrinkage during cooking at two power levels (F2 and F5).

(a) Gellan gum gel

(b) Beef burger

Fig. 11. Contribution of evaporation and dripping to water loss in the cooking of gellan gum gel and beef burger at two power levels (F2 and F5) predicted by the model.

6. Conclusions

A 2D axisymmetric computational model was developed which considers the phenomena of heat and moisture flow transfer, the deformation of meat, and the water vapour influence during the pan cooking of hamburgers. The model, fitted for the experimental results of the cooking process at the power level F2, is capable of predicting the outcomes for both burger and gel products at a higher power level, F5.

The experimental and computational results provide enhanced and in-depth understanding of hamburger pan cooking. A change in the pan temperature fundamentally affects the temperature in a thin layer of the hamburger closest to the pan, where the temperature can exceed 100 °C

once all available water has evaporated. In the rest of the hamburger, the temperature profile is independent of the pan temperature because heat is transferred from a boiling zone where the temperature does not exceed 100 °C. These considerations should be taken into account when selecting the most efficient cooking conditions. The time required to reach the recommended temperature from a microbiological point of view will be similar regardless of the pan temperature. Therefore, cooking hamburgers at a lower power level is an alternative that promotes energy consumption reduction. Additionally, it results in a juicier product as weight losses are lower when the pan temperature is decreased. These results align with culinary recommendations for meat grilling or panfrying (McGee, 2004). It is suggested to initially cook the meat over high heat to quickly achieve the Maillard reaction on

the exterior, followed by a lower heat cooking to retain more juices and preserve more of its weigh (resulting in less shrinkage) compared to cooking it at higher temperatures.

The application of the model to the cooking of gel and burger enabled the assessment of differences between two matrices of vastly different structure and composition. Furthermore, the performance of the model was validated by accounting for or disregarding the shrinkage contribution and dripping losses.

It has been demonstrated that although the higher working temperature of the pan involves higher energy consumption, the meat burger without considering the evaporation, absorbs the same amount of energy at both levels.

CRediT authorship contribution statement

E. Hernández-Alhambra: Methodology, Software, Investigation, Writing – original draft. **P. Guíu:** Methodology, Investigation, Validation. **I. Cabeza-Gil:** Conceptualization, Writing – review & editing. **A. Ferrer-Mairal:** Conceptualization, Writing – review & editing. **M.A. Martínez:** Conceptualization, Writing – review & editing. **B. Calvo:** Conceptualization, Resources, Writing – review & editing, Project administration. **J. Grasa:** Conceptualization, Methodology, Software, Writing – review & editing. **M.L. Salvador:** Conceptualization, Methodology, Resources, Investigation, Writing – original draft, Project administration.

Declaration of competing interest

The authors declare the following financial interests/personal relationships which may be considered as potential competing interests: Jorge Grasa reports financial support, administrative support, article publishing charges, and equipment, drugs, or supplies were provided by Spainish Ministry of Science and Innovation. Begona Calvo reports administrative support was provided by Government of Aragón. Jorge Grasa reports a relationship with BSH Electrodomesticos Espana S.A. that includes: funding grants.

Data availability

Data will be made available on request.

Acknowledgements

References

Ahmad, S., Khan, M.A., Kamil, M., 2015. Mathematical modeling of meat cylinder cooking. LWT Food Sci. Technol. 60, 678–683. http://dx.doi.org/10.1016/j.lwt. 2014.10.061.

AOAC, 2002. Official method 950.46. Moisture in meat. In: Official Methods of Analysis of AOAC International, sixteenth ed. Gaithersburg, MD.

Barbera, S., Tassone, S., 2006. Meat cooking shrinkage: Measurement of a new meat quality parameter. Meat Sci. 73, 467–474. http://dx.doi.org/10.1016/j.meatsci. 2006.01.011.

Bonet, J., Wood, R.D., 2008. Nonlinear Continuum Mechanics for Finite Element Analysis, second ed. Cambridge University Press, http://dx.doi.org/10.1017/ CBO9780511755446.

Chapwanya, M., Misra, N., 2015. A mathematical model of meat cooking based on polymer-solvent analogy. Appl. Math. Model. 39, 4033–4043. http://dx.doi.org/ 10.1016/j.apm.2014.12.015.

Choi, Y., Okos, M.R., 1986. Effects of temperature and composition on thermal properties of foods. J. Food Process Appl. 1, 93–101.

Dagerskog, M., 1979. Pan-Frying of Meat Patties I. A Study of Heat and Mass Transfer, Vol. 12. Lebensmittel Wissenschaft und Technologie, pp. 217–224.

Datta, A., 2007. Porous media approaches to studying simultaneous heat and mass transfer in food processes i: Problem formulations. J. Food Eng. 80, 80–95. http://dx.doi.org/10.1016/j.jfoodeng.2006.05.013.

Datta, A., Nicolaï, O., Verboven, P., Erdogdu, F., Marra, F., Sarghini, F., Koh, C., 2022. Computer-aided food engineering. Nat. Food 3, 894–904. http://dx.doi.org/ 10.1038/s43016-022-00617-5.

Dhall, A., Datta, A.K., 2011. Transport in deformable food materials: A poromechanics approach. Chem. Eng. Sci. 66, 6482–6497. http://dx.doi.org/10.1016/j.ces.2011. 09.001.

Dhall, A., Halder, A., Datta, A.K., 2012. Multiphase and multicomponent transport with phase change during meat cooking. J. Food Eng. 113, 299–309. http://dx.doi.org/ 10.1016/j.jfoodeng.2012.05.030.

Du, Q., Nekovei, R., 2005. Implementation of real-time constrained linear discriminant analysis to remote sensing image classification. Pattern Recognit. 38, 459–471. http://dx.doi.org/10.1016/j.patcog.2004.09.008.

Erdogdu, F., 2023. Mathematical modeling of food thermal processing: current and future challenges. Cur. Opin. Food Sci. 51, 101042. http://dx.doi.org/10.1016/j. cofs.2023.101042.

Erdogdu, F., Zorrilla, S.E., Singh, R.P., 2005. Effects of different objective functions on optimal decision variables: A study using modified complex method to optimize hamburger cooking. LWT Food Sci. Technol. 38, 111–118. http://dx.doi.org/10. 1016/j.lwt.2004.05.010.

Ertbjerg, P., Puolanne, E., 2017. Muscle structure, sarcomere length and influences on meat quality: A review. Meat Sci. 132, 139–152. http://dx.doi.org/10.1016/j. meatsci.2017.04.261.

Fan, Z., Cheng, P., Gao, Y., Wang, D., Jia, G., Zhang, P., Prakash, S., Wang, Z., Han, J., 2022. Understanding the rheological properties of a novel composite salecan/gellan hydrogels. Food Hydrocolloids 123, 107162. http://dx.doi.org/10.1016/j.foodhyd. 2021.107162.

Feyissa, A.H., Gernaey, K.V., Ashokkumar, S., Adler-Nissen, J., 2011. Modelling of coupled heat and mass transfer during a contact baking process. J. Food Eng. 106, 228–235. http://dx.doi.org/10.1016/j.jfoodeng.2011.05.014.

Goñi, S.M., Salvadori, V.O., 2010. Prediction of cooking times and weight losses during meat roasting. J. Food Eng. 100, 1–11. http://dx.doi.org/10.1016/j.jfoodeng.2010. 03.016.

Gulati, T., Datta, A.K., 2015. Mechanistic understanding of case-hardening and texture development during drying of food materials. J. Food Eng. 166, 119–138. http://dx.doi.org/10.1016/j.jfoodeng.2015.05.031.

Hughes, J., Oiseth, S., Purslow, P., Warner, R., 2014. A structural approach to understanding the interactions between colour, water-holding capacity and tenderness. Meat Sci. 98, 520–532. http://dx.doi.org/10.1016/j.meatsci.2014.05.022.

Khan, M.I.H., Joardder, M.U.H., Kumar, C., Karim, M.A., 2016. Multiphase porous media modelling: A novel approach to predicting food processing performance. Crit. Rev. Food Sci. Nutr. 58, 528–546. http://dx.doi.org/10.1080/10408398.2016. 1197881.

Kondjoyan, A., Oillic, S., Portanguen, S., Gros, J.B., 2013. Combined heat transfer and kinetic models to predict cooking loss during heat treatment of beef meat. Meat Sci. 95, 336–344. http://dx.doi.org/10.1016/j.meatsci.2013.04.061.

Liu, Z., Shaposhnikov, M., Zhuang, S., Tu, T., Wang, H., Wang, L., 2023. Growth and survival of common spoilage and pathogenic bacteria in ground beef and plant-based meat analogues. Food Res. Int. 164, 112408. http://dx.doi.org/10.1016/j. foodres.2022.112408.

McGee, H., 2004. On Food and Cooking: The Science and Lore of the Kitchen, second ed. Collier Books, Scribner, New York, pp. 147–154.

Morris, E.R., Nishinari, K., Rinaudo, M., 2012. Gelation of gellan - a review. Food Hydrocolloids 28, 373–411. http://dx.doi.org/10.1016/j.foodhyd.2012.01.004.

Moya, J., Lorente-Bailo, S., Salvador, M., Ferrer-Mairal, A., Martínez, M., Calvo, B., Grasa, J., 2021. Development and validation of a computational model for steak double-sided pan cooking. J. Food Eng. 298, 110498. http://dx.doi.org/10.1016/j. jfoodeng.2021.110498.

Myhrvold, N., Young, C., Bilet, M., Smith, R.M., 2011. Modernist Cuisine: The Art and Science of Cooking. Vol 3, first ed. Cooking Lab, Bellevue, WA, pp. 72–79.

Nelson, H., Deyo, S., Granzier-Nakajima, S., Puente, P., Tully, K., Webb, J., 2020. A mathematical model for meat cooking. Eur. Phys. J. Plus 135, 4033–4043. http://dx.doi.org/10.1140/epjp/s13360-020-00311-0.

Nesvadba, P., 2014. Thermal properties of unfrozen foods. In: Engineering Properties of Foods, fourth ed. CRC Press, pp. 223–246. http://dx.doi.org/10.1201/b16897-8.

Nursten, H.E., 2005. The Maillard Reaction: Chemistry, Biochemistry and Implications. Royal Society of Chemistry, Cambridge.

Onopiuk, A., Kołodziejczak, K., Szpicer, A., Wojtasik-Kalinowska, I., Wierzbicka, A., Półtorak, A., 2021. Analysis of factors that influence the pah profile and amount in meat products subjected to thermal processing. Trends Food Sci. Technol. 115, 366–379. http://dx.doi.org/10.1016/j.tifs.2021.06.043.

Oroszvári, B.K., Bayod, E., Sjöholm, I., Tornberg, E., 2005a. The mechanisms controlling heat and mass transfer on frying of beefburgers, part 2: The influence of the pan temperature and patty diameter. J. Food Eng. 71, 18–27. http://dx.doi.org/10. 1016/j.jfoodeng.2004.10.013.

Oroszvári, B.K., Bayod, E., Sjöholm, I., Tornberg, E., 2006. The mechanisms controlling heat and mass transfer on frying of beefburgers, iii. mass transfer evolution during frying. J. Food Eng. 76, 169–178. http://dx.doi.org/10.1016/j.jfoodeng.2005.05.018.

Oroszvári, B.K., Sjöholm, I., Tornberg, E., 2005b. The mechanisms controlling heat and mass transfer on frying of beefburgers, i. the influence of the composition and comminution of meat raw material. J. Food Eng. 67, 499–506. http://dx.doi.org/10.1016/j.jfoodeng.2004.05.017.

Ou, D., Mittal, G.S., 2006. Double-sided pan-frying of unfrozen/frozen hamburgers for microbial safety using modelling and simulation. Food Res. Int. 39, 133–144. http://dx.doi.org/10.1016/j.foodres.2005.06.009.

Ou, D., Mittal, G., 2007. Single-sided pan frying of frozen hamburgers with flippings for microbial safety using modeling and simulation. J. Food Eng. 80, 33–45. http://dx.doi.org/10.1016/j.jfoodeng.2006.03.033.

Pan, Z., Singh, R.P., 2001. Physical and thermal properties of ground beef during cooking. LWT Food Sci. Technol. 34, 437–444. http://dx.doi.org/10.1006/fstl.2001.0762.

Pan, Z., Singh, R., Rumsey, T., 2000. Predictive modeling of contact-heating process for cooking a hamburger patty. J. Food Eng. 46, 9–19. http://dx.doi.org/10.1016/S0260-8774(00)00063-7.

Shilton, N., Mallikarjunan, P., Sheridan, P., 2002. Modeling of heat transfer and evaporative mass losses during the cooking of beef patties using far-infrared radiation. J. Food Eng. 55, 217–222. http://dx.doi.org/10.1016/S0260-8774(02)00066-3.

Sohail, A., Al-Dalali, S., Wang, J., Xie, J., Shakoor, A., Asimi, S., Shah, H., Patil, P., 2022. Aroma compounds identified in cooked meat: A review. Food Res. Int. 157, 111385. http://dx.doi.org/10.1016/j.foodres.2022.111385.

Straub, J., 1985. In: Haar, Von L., Gallagher, J.S., Kell, G.S. (Eds.), NBS/NRC Steam Tables. Hemisphere Publishing Corp., Washington-New York-London, http://dx.doi.org/10.1002/cite.330570931, 1. Aufl. XII, 320 S. geb. 1984. Chemie Ingenieur Technik 57, 812.

Szpicer, A., Wierzbicka, A., Pótorak, A., 2022. Optimization of beef heat treatment using cfd simulation: Modeling of protein denaturation degree. J. Food Eng. 45, e14014. http://dx.doi.org/10.1111/jfpe.14014.

Thiffeault, J.L., 2022. The mathematics of burger flipping. Physica D 439, 133410. http://dx.doi.org/10.1016/j.physd.2022.133410.

Tornberg, E., 2005. Effects of heat on meat proteins - implications on structure and quality of meat products. Meat Sci. 70, 493–508. http://dx.doi.org/10.1016/j.meatsci.2004.11.021.

Tornberg, E., 2013. Engineering processes in meat products and how they influence their biophysical properties. Meat Sci. 95, 871–878. http://dx.doi.org/10.1016/j.meatsci.2013.04.053.

USDA, 2016. Food safety and inspection service. ground beef and food safety. URL https://www.fsis.usda.gov/food-safety/safe-food-handling-and-preparation/meat/ground-beef-and-food-safety. (Last accessed 21 July 2023).

van der Sman, R., 2007. Moisture transport during cooking of meat: An analysis based on flory–rehner theory. Meat Sci. 76, 730–738. http://dx.doi.org/10.1016/j.meatsci.2007.02.014.

van der Sman, R., 2015. Biopolymer gel swelling analysed with scaling laws and flory–rehner theory. Food Hydrocolloids 48, 94–101. http://dx.doi.org/10.1016/j.foodhyd.2015.01.025.

Vaskoska, R., Ha, M., Tran, H., Khoshelham, K., White, J., Warner, R., 2020. Evaluation of 3d laser scanning for estimation of heating-induced volume shrinkage and prediction of cooking loss of pork cuboids compared to manual measurements. Food Bioprocess Technol. 13, 938–947. http://dx.doi.org/10.1007/s11947-020-02421-0.

Vu, G., Zhou, H., McClements, D.J., 2022. Impact of cooking method on properties of beef and plant-based burgers: Appearance, texture, thermal properties, and shrinkage. J. Agric. Food Res. 9, 100355. http://dx.doi.org/10.1016/j.jafr.2022.100355.

Vujosevic, L., Lubarda, V.A., 2002. Finite-strain thermoelasticity based on multiplicative decomposition of deformation gradient. Theor. Appl. Mech. 28, 379–399. http://dx.doi.org/10.2298/TAM0229379V.

Zheng, C., Sun, D.W., Zheng, L., 2007. Predicting shrinkage of ellipsoid beef joints as affected by water immersion cooking using image analysis and neural network. J. Food Eng. 79, 1243–1249. http://dx.doi.org/10.1016/j.jfoodeng.2006.04.010.

Zorrilla, S.E., Singh, R., 2003. Heat transfer in double-sided cooking of meat patties considering two-dimensional geometry and radial shrinkage. J. Food Eng. 57, 57–65. http://dx.doi.org/10.1016/S0260-8774(02)00273-X.